JOURNAL OF SYNCHROTRON RADIATION

ISSN 1600-5775

The U125 insertion device beamline at the Metrology Light Source

Alexander Gottwald,* Hendrik Kaser and Michael Kolbe

Physikalisch-Technische Bundesanstalt, Abbestraße 2-12, Berlin 10587, Germany.
*Correspondence e-mail: alexander.gottwald@ptb.de

Received 8 October 2018
Accepted 28 December 2018

Edited by Y. Amemiya, University of Tokyo, Japan

Keywords: undulator beamline; extreme ultraviolet; radiometry; spectral purity.

At the Metrology Light Source, an electron storage ring dedicated to metrological applications, the U125 insertion device beamline utilizes undulator radiation for various applications over a broad spectral range. Using a hybrid normal-incidence and grazing-incidence in-vacuum switchable plane-grating monochromator, a spectral region ranging from the near-infrared to soft X-ray is covered. The beamline is dedicated to surface-analytical methods, *e.g.* ellipsometry, photoelectron spectroscopy or photoemission tomography. The traceability of radiometric quantities, *i.e.* quantitative determination of the available radiant power (or photon flux), is required for some of these applications to support the metrological aspect of the measurements. In particular, attention is paid to the suppression of unwanted spectral contributions from higher diffraction orders, and to the monitoring of the radiation intensity during the measurements. With the results from the beamline commissioning, an uncertainty budget for all relevant radiometric quantities was established.

1. Introduction

The Metrology Light Source (MLS) in Berlin–Adlershof is the electron storage ring of the Physikalisch-Technische Bundesanstalt (PTB), Germany's national metrology institute. The MLS provides synchrotron radiation for radiometric and analytical measurements in the spectral range from the terahertz regime to the extreme ultraviolet (Gottwald *et al.*, 2012). The ring has a circumference of 48 m and can be operated at a maximum electron energy of 630 MeV with a maximum beam current of 200 mA. User operation of the MLS started in 2008, and its size and design resemble a second-generation synchrotron light source (*e.g.* it has only one long straight section available for an insertion device). A total of seven beamlines, which were set up sequentially from 2008 to 2012, are currently available for measurements.

PTB has more than 30 years of experience in the use of synchrotron radiation for metrology (Beckhoff *et al.*, 2009). In the beginning, the measurements were focused on basic radiometric methods using ultraviolet (UV), vacuum-ultraviolet (VUV) and extreme-ultraviolet (EUV) radiation from the former BESSY I electron storage ring. With the opening of the BESSY II facility in 1999, the spectral range was extended towards the X-ray regime. Since then, the scope of methods has continuously been expanded to analytical methods such as reference-free X-ray fluorescence analysis (Kolbe *et al.*, 2009; Beckhoff, 2008; Lubeck *et al.*, 2013) and X-ray scattering methods (Garcia-Diez *et al.*, 2015). For these applications, PTB focuses on the metrological context, *i.e.* the aspect of traceability of quantitative measurements to primary standards.

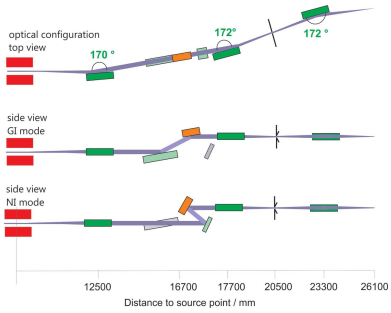

Table 1
Parameters of the optical elements of the MLS IDB.

Optical element	M1	M2a	M2b	G1 GI 1200Ru	G2 NI 600B4C	G3 NI 600Al	M3	M4
Shape	Toroid	Plane	Plane	Plane	Plane	Plane	Cylinder	Toroid
Optical surface size (mm)	30 × 200	30 × 200	∅ 20	30 × 100	23 × 23	23 × 23	50 × 130	40 × 30
Coating	Rh	Au	Pt	Ru	B_4C	Al + MgF_2	Au	Au
Deflection angle	10°	–	20°	–	–	–	8°	8°
Meridional radius (mm)	107600	∞	∞	∞	∞	∞	∞	45160
Sagittal radius (mm)	2180	∞	∞	∞	∞	∞	391	220
Line density (mm^{-1})	–	–	–	1200	600	600	–	–

Extending the analytical capabilities into the VUV enables us to determine material-specific constants and properties over a broad spectral range and therefore gain a deeper understanding of the composition–property relation. These analytical measurements benefit from high photon fluxes by allowing data collection with sufficient statistics in reasonably short measurement times. Thus, the MLS U125 undulator emission is used with a dedicated insertion device beamline (IDB) with regards to spectroscopic analytics. For standard radiometric measurements in the VUV and EUV spectral ranges (*e.g.* for detector calibration and reflectance characterization of optical components), the MLS bending magnet beamlines are still favoured, since their (lower) radiant power commonly results in higher stability for a high-precision calibration measurement (Gottwald *et al.*, 2010; Laubis *et al.*, 2016). The U125 undulator emission covers the spectral range from the soft X-ray (4.4 nm or 284 eV, *i.e.* the carbon *K*-edge) to the near-infrared (1300 nm or 0.95 eV). Besides this spectral broadness, spectral purity, stability (*i.e.* reproducibility of measurements) and reliable intensity monitoring have been substantial design criteria for the beamline.

2. Design and layout

2.1. Undulator source parameters

In 2012, in the long straight section available at the MLS, a permanent-magnet-type undulator with 125 mm full period (U125) was installed. It is 4230 mm in length and has 30 full field periods. The magnetic field strength is changed by moving the undulator gap between 180 mm and 34.4 mm which results in a maximum undulator K parameter of $K = 7.5$. The value of the undulator strength parameter K describes the nature of the electron motion, *i.e.* whether the oscillation amplitude induced by the magnetic field strength is small enough to result in an interference pattern for the emitted radiation (undulator mode, $K \ll 1$) (Motz *et al.*, 1953). Changing the K parameter in the given range shifts the first harmonic emission from about 65 nm ($K = 0.1$) to 1300 nm ($K = 7.5$) when the MLS is operated at its maximum electron energy of 630 MeV. In the upper K limit, however, the emission spectrum is rather continuous, with only slight remaining modulations (wiggler mode) with sufficiently intense photon emission down to wavelengths of 4.4 nm. In undulator mode, the spectral width $\Delta E/E$ of the first harmonic is approximately given by $1/N$ with N being the number of full periods (*i.e.* $N = 30$ in our case). Thus, in routine operation, the undulator will be tuned parallel to the monochromator in order to change the wavelength. In the MLS, the electron beam size in the undulator (source size) is typically around 270 µm vertically and 450 µm horizontally (Klein *et al.*, 2008). The divergence of the radiation increases from about 100 µrad in undulator mode to a few mrad in wiggler mode. The polarization of the emitted radiation is linear horizontal to a high degree (Neumann *et al.*, 2014). Besides the monochromator beamline described in this work, the undulator radiation can be used in a direct as well as a 10°-deflected beamline branch for measurements without need for further monochromatization beyond the natural undulator linewidth (Stellmer *et al.*, 2018).

2.2. Overall beamline design

The basic optical scheme of the IDB is shown in Fig. 1 and the basic optical element parameters are given in Table 1. The beamline is based on the collimated plane-grating monochromator (cPGM) design (Follath & Senf, 1997). The overall length of the beamline from the centre of the undulator (as the source point) to the focal point is 26.1 m. In the undulator

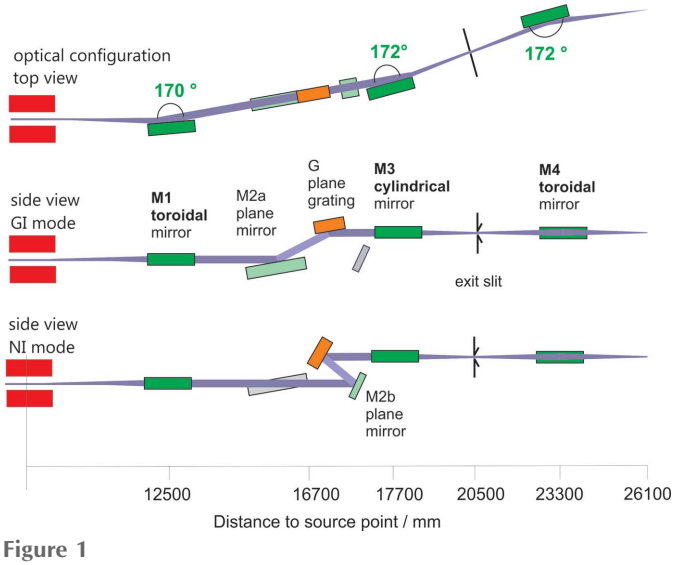

Figure 1
Schematic optical layout of the IDB at the PTB Metrology Light Source. GI and NI modes can be switched under vacuum simply by moving the optical elements of the monochromator.

front end, a set of knife-edge precision apertures can be used to crop the beam. The first mirror (M1) is located at a distance of 12.5 m from the source point. M1 is of toroidal shape which creates a parallel beam in the dispersive (vertical) direction, whereas in the non-dispersive (horizontal) direction the source is imaged to the exit slit. It deflects the beam by 10° and has a rhodium-coated surface. The plane-grating monochromator is described in detail in Section 2.3. Behind the monochromator, the (dispersed) radiation is focused on the exit slit by a cylindrical mirror (M3), so that the exit-slit position is in the vertical as well as the horizontal focus. The imaging conditions are given by the optical path lengths so that the source is demagnified 1:1.56 in the horizontal and 1:4.46 in the vertical (dispersive) directions. The toroidal mirror (M4) images the exit slit to the beamline focus without any demagnification (1:1). The optical elements accept a radiation cone of 1.4 mrad full divergence from the undulator source. Order-sorting filters (Section 2.4) and beamsplitter intensity monitors (Section 2.5) are located between the exit slit and M4. This part of the beamline also comprises a differentially pumped gas ionization cell which is designed to be used for spectral filtering (Section 2.4) as well as intensity measurements (Section 2.5).

2.3. cPGM NI–GI monochromator

Plane-grating monochromators for synchrotron radiation developed from the original Petersen SX700 design (Petersen & Baumgärtel, 1980). This design is composed of a plane mirror (M2a) and a plane grating (G) by which the angle of incidence and diffraction of the grating are varied with the wavelength in order to keep the fixed-focus condition (constant c_{ff} factor) fulfilled. The spectral range covered depends on the angular range for the mirror and grating rotation. The grazing-incidence (GI) part of the monochromator is designed for a maximum angle of 35° for the grating and 29° for the mirror with respect to the horizontal plane. This results in a maximum wavelength of about 120 nm (10 eV) in this configuration. However, for wavelengths larger than 50 nm (photon energies below 25 eV), the higher diffraction orders from the grating cannot be effectively suppressed by filters (see Section 2.4), which contradicts the demand for high spectral purity. To extend the spectral capabilities, a normal-incidence (NI) option using the mirror M2b with a constant deviation angle of 20° in combination with an NI grating is applied. This option has the advantage of naturally suppressing higher-order diffraction from the grating due to the vanishing reflectance of short-wavelength radiation under near-normal angles of incidence. The combination of a NI and GI monochromator in one beamline has already been realized with different designs and geometry (Derossi *et al.*, 1995; Flechsig *et al.*, 2001; Cimino & Lama, 2001; Nannarone *et al.*, 2004). However, the chosen cPGM design promises a solution with only minor changes to the proven SX700 design and has been successfully operated previously (Flechsig, 2004). The NI–GI monochromator used for the IDB contains four mounting slots for different gratings. These slots can be freely used either with an NI or GI grating which comes with individual adapter frames. In the current setup, two normal-incidence laminar profile gratings with 600 lines mm^{-1} line density are in use (with an Al + MgF_2 coating for $\lambda > 120$ nm, and B_4C coating for 40 nm $< \lambda <$ 145 nm) together with one GI 1200 lines mm^{-1} blazed profile grating (with a Ru coating for 4.4 nm $< \lambda <$ 50 nm). For GI mode an Au-coated plane mirror is used, whereas for NI mode a Pt-coated plane mirror is used. To switch between the GI and NI modes, the GI mirror has to be retracted from the beam path, and the respective grating must be moved in. The mechanical setup (in particular, the grating rotation axis) is used by both modes. Optical angle-encoders with a resolution of 0.1 µrad ensure the required accuracy in the adjustment of the rotary axes.

Table 2
Upper limits for the detection of false light contributions (integral higher grating orders) for the three gratings of the NI–GI monochromator, measured at the filter transmission edges of the respective wavelength sub-ranges.

Grating	Filter	Wavelength (nm)	Configuration number	Stray-light and higher-order contribution (%)
GI 1200Ru	–	4 to 11	(i)	Not determined
	Be	11 to 22	(ii)	0.2
	Al	17 to 34	(iii)	0.8
	Mg	25 to 49	(iv)	0.3
NI 600B4C	–	40 to 60	(v)	0.4
	Ne	58 to 110	(vi)	8.7
	Ar	80 to 145	(vii)	0.05
NI 600Al	Ne	58 to 110	(viii)	0.4
	Ar	80 to 145	(ix)	0.01
	MgF_2	115 to 225	(x)	<0.01
	Suprasil	170 to 310	(xi)	<0.01
	WG295	300 to 600	(xii)	<0.01
	GG395	400 to 800	(xiii)	<0.01

2.4. Filters for spectral purity

For metrological applications, the spectral purity of the monochromated radiation is key in determining absolute radiant power (or photon flux) by means of non-dispersive detector standards (*e.g.* calibrated semiconductor photodiodes). To suppress higher-order diffraction from the grating to a sub-percentage level, different filtering methods are realized in the beamline for different spectral sub-ranges. The IDB optical configurations (grating and filter settings) are summarized in Table 2. For the range from visible down to 115 nm, a set of optical (bulk) filters (GG395, WG295, Suprasil, MgF_2) are used. Between 120 nm and 40 nm, the differentially pumped gas absorption cell installed in the beamline can be used, which can be filled with various (noble) gases up to 0.1 mbar pressure. The absorption cell itself is the beamline segment between the exit slit and M4 (refocusing) mirror, limited upstream and downstream by a set of nozzle apertures with differential pumping by a total of eight turbomolecular pumps. Similar concepts were already known from beamlines at other facilities (*e.g.* Suits *et al.*, 1995; Mercier *et al.*, 2000).

However, in this wavelength range, the use of the NI 600 lines mm^{-1} B_4C grating already offers a significant reduction of short-wavelength contributions in comparison with the GI mode, as the NI reflectance of B_4C rapidly decreases below 50 nm. From 50 nm down to 11 nm (in the GI mode of the monochromator), filter foils (Mg, Al, Be) with thicknesses of only a few 100 nm are used. For wavelengths shorter than the Be filter edge ($\lambda < 11.4$ nm), higher-order suppression through the proper choice of c_{ff} parameter (*i.e.* setting of plane mirror/grating angle combination for a certain wavelength) in combination with the sharp cut-off of the photon flux at the carbon edge is used.

2.5. Intensity monitoring

Synchrotron beamlines commonly offer basic techniques to measure and monitor the photon flux, *e.g.* by gold meshes. However, these techniques, although robust in daily use, are limited regarding their use over a broad spectral range. They are similarly limited in their stability and, in particular, their absolute calibration. For an absolute measurement, a traceably calibrated detector must be used, *i.e.* it must be calibrated referring to a radiometric primary standard. Absolute and traceable calibration of radiation detectors regarding their spectral responsivity is one of the core competences of the PTB in synchrotron-radiation-based radiometry (Gottwald *et al.*, 2006). With a calibrated photodiode as a transfer (secondary) standard, the intensity monitors can be calibrated subsequently. At the IDB, different monitors are available for different spectral sub-ranges. In the short-wavelength regime, the photoemission current from the M4 mirror is used: its metallic surface is electrically insulated and a voltage of +50 V can be applied. Naturally, this method is restricted to photon energies sufficient for the photoelectric effect (*i.e.* $\lambda <$ 230 nm). It is very sensitive to higher-order contributions and the position of the beam on the M4 surface, since the electron collection efficiency varies over the surface due to, for example, irradiation-induced carbon contamination. For wavelengths below 200 nm, the gas absorption cell (see Section 2.4) can be operated as an ionization monitor, since it has a set of electrodes inside to which a voltage up to 500 V can be applied. If the gas pressure is measured absolutely by a calibrated spinning rotor gauge, and since the geometry parameters are known, the system can even act directly as an absolute measuring device in certain wavelength regions based on the known cross sections for atomic photoionization, as demonstrated by photoionization-based monitor systems used for free-electron laser radiaton beamlines (Tiedtke *et al.*, 2008). For the long-wavelength range, $\lambda > 120$ nm, two beam-splitter systems (either with a Suprasil or a MgF_2 plate) are in use which reflect part of the beam to a photodiode. Since the angle of the reflectance plate is fixed, the signal varies with changing beam positions, thus leading to a limited temporal stability. As an additional intensity monitor, the precision knife-edge blades in the undulator front-end can be operated with a bias voltage to collect photoelectrons emitted due to irradiation by the outer (cut) parts of the undulator beam. However, this monitoring is practically limited to single undulator settings and, thus, wavelengths, since the undulator (gap) has to be tuned when the wavelength is changed.

3. Measurements of characteristics and performance

3.1. Beam geometry

The geometry of the beamline focal spot is defined by the toroidal mirror M4 which images the exit slit to the beamline focus. The exit slit unit consists of a pair of high-precision blades in the dispersive direction, which can be moved with a parallelism better than 1 µm. To adjust the beam size in the horizontal direction, two additional blade apertures are mounted. The exit slit is imaged 1:1 by M4 so that the focal spot size changes with the slit opening. However, the minimum beam size is limited by diffraction at the blade edges, while the maximum horizontal spot size is given by the image of the source itself. Practically, we found that the focus can be set between 0.1 mm and 1.5 mm. The focusing is demonstrated in Fig. 2 which shows the vertical beam size versus the distance from the focus position.

To determine the focus position, a CCD camera was moved along the beam path. The exit slit unit was set to a height of 100 µm (vertical) and a width of 1 mm (horizontal). The zero position was adjusted according to the calculated focus position (26.1 m from the source point). The measurement is shown for three different wavelengths from different optical configurations (as will be described in the next subsection). It can be seen that the focal position and size are independent of these settings; however, the shape of the curve changes slightly due to the different grating alignment and, moreover, because of the source size and the divergence of the undulator radiation which changes with the different K parameters for the different wavelengths. Due to small misalignments, the sagittal and meridional foci of the M4 toroid are not exactly in the

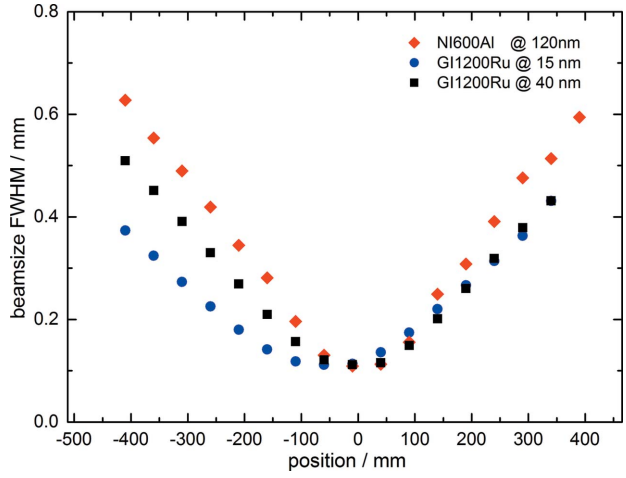

Figure 2
Full width at half-maximum vertical beam size around the beamline focal position taken at wavelengths of 15 nm (blue circles), 40 nm (black squares) and 120 nm (red diamonds). The zero position corresponds to the ideal position calculated from the design (26.1 m from the source point according to Fig. 1).

same position. In practice, the vertical focus position is used in most cases for the position of the experimental endstations.

3.2. Photon flux and higher orders

Fig. 3 shows the available photon flux at the IDB, measured with a 0.5 mm exit-slit opening and normalized to 100 mA of stored electron current in the MLS. The horizontal (non-dispersive) apertures were fully opened by 2 mm so that the full beam width was taken into account. The MLS was operated at the maximum electron energy of 630 MeV, and the undulator K parameter was always set to the maximum emission of the harmonics at the respective wavelength, *i.e.* the undulator and monochromator were moved simultaneously. For the absolute flux determination, a traceably calibrated photodiode was used. In the GI mode of the monochromator, the c_{ff} parameter was set to 2. The different beamline settings (undulator harmonics/wiggler mode, grating and filter) are indicated by the different colours in the graph. The Roman numerals of the configuration correspond to those in Table 2. From Fig. 3, it can be seen that the IDB offers photon fluxes larger than 10^{12} s^{-1} in most wavelength ranges provided. The obvious discontinuities in the GI range are due to the different filter transmissions (Table 2). On the short-wavelength limit of the spectral range covered by the IDB, the photon flux drastically decreases due to the undulator characteristics. It also decreases because of the reflectance of the optical elements under the chosen deflection angles, in particular due to carbon absorption on contaminated surfaces. Thus, the short-wavelength limit for useable radiation is the carbon K-edge at a photon energy of 284 eV (4.4 nm).

The suppression of the higher-order grating diffraction by the filters used was determined by measuring the remaining signal from a calibrated photodiode behind the filter at wavelengths just below the absorption edge of the respective filter (Table 2). Since this method is at least limited by the noise in signal detection, it only gives an upper limit for any kind of off-wavelength radiation passing through the filter. Additional measurements were made by means of a CCD grating spectrograph to validate that higher-order diffraction contributions are suppressed.

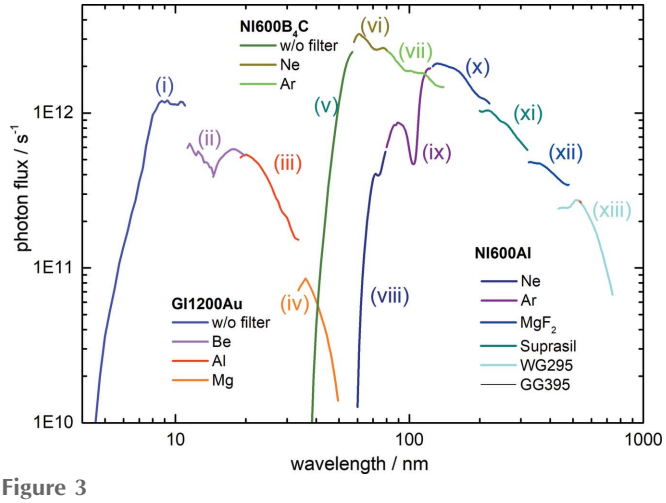

Figure 3
Measured photon flux at the IDB for different optical configurations (see Table 2) in the wavelength range from 4.4 nm to 800 nm. All curves are normalized to 100 mA of MLS-stored electron current and measured with a constant exit slit of 0.5 mm, with a corresponding bandwidth according to Fig. 4.

3.3. Spectral resolution

The resolution of the IDB is limited by the size of the source image in the exit-slit plane. With regards to the conditions available at the MLS, the beamline was designed for purity and stability and reaches an only moderate spectral resolution: the vertical source size (Section 2.1) is relatively large compared with other recent (third-generation) synchrotron radiation sources and the total length is restricted due to the floor space available in the MLS experimental hall. The imaging ratios are near unity, and mirror curvatures have to be relatively strong (*i.e.* small radii, see Table 1), resulting in relatively large optical aberration errors. Basically, the spectral resolution can be set by the exit-slit opening. However, if the optical limit (*i.e.* the size of the imaged source in the exit slit) is reached, further reduction of the slit size will not further increase the resolution. This is demonstrated in Fig. 4, where the measured wavelength resolution is shown versus the exit-slit height for the different gratings. The resolution here was measured for the NI gratings at the 123.6 nm absorption resonance of atomic krypton by registering the reference photodiode current behind the absorption cell while scanning the monochromator wavelength. The spectral resolution was determined as the full width at half-maximum of the measured absorption lines. Since the natural line widths are much smaller than the wavelength resolution, their effect is neglected. It can be seen that down to a slit height of about 100 µm the resolution follows a linear slope. Below 100 µm, the curve saturates to a value of $\Delta\lambda$ = 0.09 nm for the NI600B4C and $\Delta\lambda$ = 0.05 nm for the NI600Al grating, resulting in a resolving power of $R = \lambda/\Delta\lambda$ = 1370 and R = 2470, respectively. The different values achieved might be

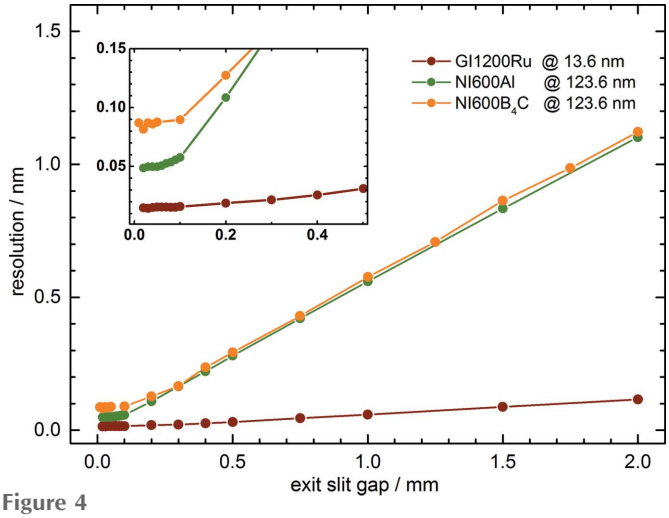

Figure 4
Spectral resolution of the IDB as a function of the exit-slit opening at 13.6 nm for the GI1200Ru grating and 123.6 nm for the NI600 gratings, measured using Kr gas absorption resonances.

explained by a slight optical misalignment of the B4C grating: even a small angular deviation leads to an off-axis beam path for the strongly curved M3 mirror, which then induces stronger optical aberrations to the image at the exit-slit position. For the GI grating, the atomic Kr resonance at 13.6 nm was used, leading to a resolution of $\Delta\lambda = 0.015$ nm ($R = 840$).

3.4. Wavelength calibration and stability

The monochromator wavelength setting is determined by the angular position of the grating and additionally for the GI mode of the plane mirror. The position is measured by two independent angle encoders, from each of which the mean value is taken into account. To define the wavelength scale, several photoabsorption resonances from noble gases are used, for which the wavelengths are well known (Kramida *et al.*, 2014). These measurements were taken into account to determine the overall wavelength uncertainty (0.002 nm for the GI1200Ru grating and 0.005 nm for the two NI600 gratings).

During the beamline operation, the wavelength scale is checked at least on a daily basis. For the NI mode of the monochromator, the zero order is determined and (if needed) the wavelength scale is corrected for the measured offset. For the GI scale, where (due to the more complicated dependence of the wavelength from the grating and mirror position) the full calibration procedure is much more time-consuming, the relative position of the Al absorption edge at 17.1 nm is used. Deviations smaller than 10 pm were accepted with regard to the 15 pm spectral resolution, but larger discrepancies require a complete re-calibration. Fig. 5 gives examples of results for deviation from the median for a number of repeated measurements of the zero-order position (for NI) and the Al absorption edge position (for GI) over a (irregular) time span of a few months duration. The GI [Fig. 5(*a*)] and NI [Fig. 5(*b*)] measurements were uncorrelated regarding their number of measurements. In particular for the GI case it can be seen that the deviation underwent certain stepwise changes. These are suspected to depend on a change of the electron beam conditions in the MLS storage ring which may occur (*e.g.* for different operation modes of the ring). However, even with these steps, the overall reproducibility of the wavelength scale lies within 0.01 nm (GI) and 0.015 nm (NI), respectively.

3.5. Monitor stability

The different intensity monitors described in Section 2.5 are used for the normalization of measurements to the incident intensity. This is greatly needed since the MLS is operated in decay mode with a permanently decreasing electron current and, thus, photon intensity. Moreover, the photon flux depends on the electron beam size and position (as the beamline transmittance is geometry dependent), the adjustment of the optical elements, and (on a long-term scale) the contamination-induced absorbance of radiation on the reflecting surfaces. However, for some types of measurements it might be sufficient to achieve relative normalization, *e.g.* for any radiometric approach the absolute value must be determined. Thus, the monitors should be absolutely calibrated with regard to a radiometric standard. However, the temporal stability of the monitor signal is limited since the monitor's dependencies on any changes (*e.g.* beam geometry) are different than for the total flux in the beamline focus. Fig. 6 shows an example of the relative changes of the monitor signals for 1 h (normalized to the individual start signal at $t = 0$), normalized to the signal from an absolutely calibrated photodiode near the beamline focus. For comparison, besides the M4 mirror current (red), the gas ionization cell (blue) and the beam splitter monitor (green), also the relative changes in the current of the electrons stored in the MLS (black) and the photoemission current from the precision knife-edge blades (magenta) are depicted. The data points are connected with lines to guide the eye. The measurements were conducted at a wavelength of 80 nm [*i.e.* configuration (vii)] except for the quartz beamsplitter where 200 nm [configuration (xi)] was chosen for a separate recording. The result shown was obtained under routine operation of the MLS. It can be seen

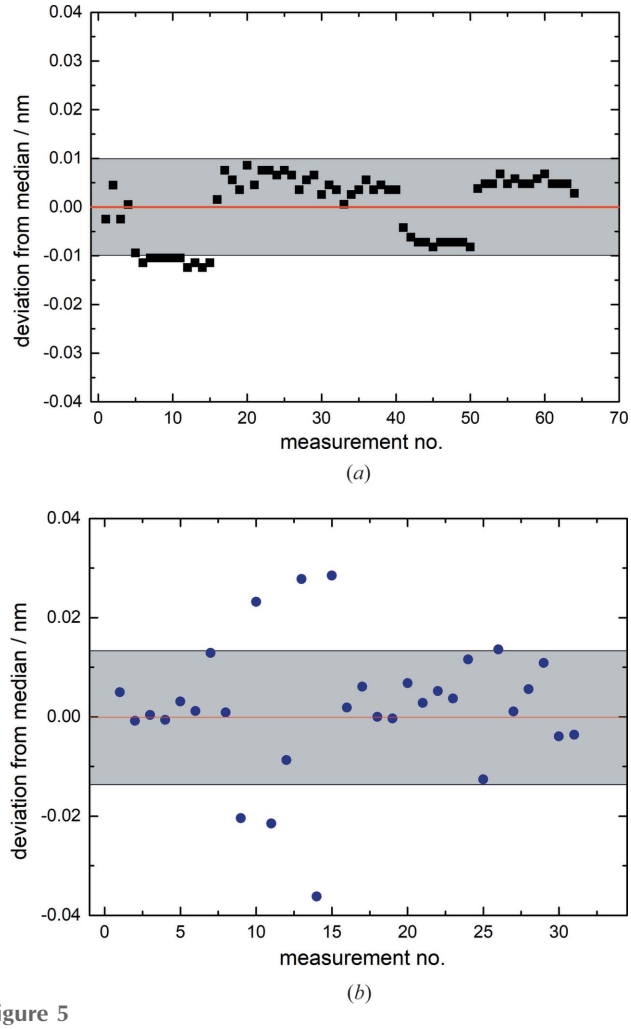

Figure 5
Stability of wavelength calibration in (*a*) GI mode (black squares) and (*b*) NI mode (blue dots). The (absolute) deviation from the long-term median for the measured Al absorption edge (17.1 nm) in GI mode and the zero-order central position in NI mode are shown. The measurements have been conducted independently and with no fixed time correlation over a temporal range of a few months.

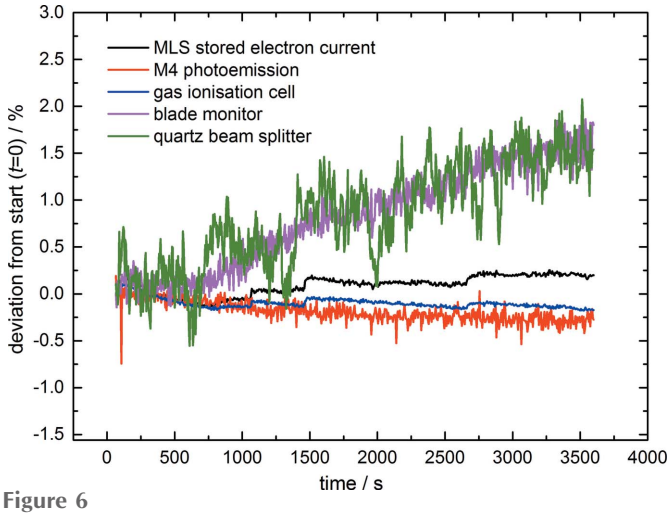

Figure 6
Stability of the different intensity monitors at IDB relative to an absolutely calibrated photodiode in the beamline focus for the duration of 1 h. The measurements were conducted at a 80 nm wavelength except for the quartz beamsplitter which was carried out at 200 nm in a separate measurement.

that the gas ionization cell and the M4 mirror photoemission monitor show the highest relative stability (better than $\pm 0.2\%$), whereas the quartz beamsplitter has the largest drift and noise, ending up with a deviation of +1.5%.

4. Applications and scientific highlights

For spectroscopic applications, *e.g.* ellipsometry (Neumann *et al.*, 2014) and photoelectron spectroscopy (Roth *et al.*, 2014, 2015, 2016, 2018), the main advantage of the beamline is its extremely broad spectral range. For photoelectron spectroscopy, the overlap between ultraviolet photoelectron spectroscopy (UPS) for surface-state and valence-band characterization and X-ray photoelectron spectroscopy (XPS) for inner-shell excitations is valuable. In contrast, for spectroscopic ellipsometry, the overlap to the ultraviolet and visible range is of particular importance as this also has the possibility for a comparison with laboratory-based instruments. Furthermore, it is well suited for experiments combining methods in different photon-energy regimes, for example, UV radiation ageing and UPS/XPS diagnostics (Darlatt *et al.*, 2016).

The spectral purity delivered by the beamline is of particular importance for the absolute photon-flux determination, since any calibrated non-dispersive detector will be sensitive to spectrally false radiation parts (*e.g.* from higher grating orders). Even for relative (normalization) measurements, this is of importance as the ratio between at-wavelength and out-of-band radiation parts cannot be regarded as a constant. This ability for correct normalization is essential for absolute measurements, *e.g.* of absolute photoionization cross sections (Schaefer *et al.*, 2018), but also for methods like photoemission tomography which unveils 3D electron orbitals by angular-resolved measurements of photoelectron emissions (Weiß *et al.*, 2015; Lüftner *et al.*, 2017).

Table 3
Exemplary uncertainty contributions for the photon-flux measurement at 200 nm and 20 nm wavelengths.

	Standard relative measurement uncertainty (%)	
Quantity	200 nm	20 nm
Reference detector calibration	1.1	1.5
Calibration drift/ageing†	3.0	1.3
Measured photocurrent	<0.1	<0.1
Wavelength	<0.1	<0.1
Spectral bandwidth	<0.1	<0.1
Stray-light, higher diffraction orders	<0.1	0.8
Monitor stability (1 h)	1.5	0.3
Resulting total photon flux	3.5	2.2

† Based on experience for a typical one-year recalibration cycle.

Examples of uncertainty contributions of the photon flux for a practical measurement (flux measurement by a monitor) are given in Table 3 for two wavelengths, 200 nm in NI mode and 20 nm in GI mode. Using spectrally purifying filters, unwanted out-of-band radiation gives only a minor contribution to the total uncertainty. Aside from the uncertainty from the primary calibration of the detector in use, the most relevant uncertainty contributions arise from stability issues. On the one hand, the reference detector itself will undergo changes (*e.g.* irradiation-induced degradation) leading to a deviation from the initial (calibrated) spectral responsivity (calibration drift). On the other hand, the respective intensity monitor has only limited stability with time (Fig. 6), thus the uncertainty grows with the duration of the measurement. The values given in Table 3 can only be regarded as examples, since they will depend on, for example, the irradiation dose applied to the reference detector (irradiation ageing) and the stability of the MLS operation (electron beam drift). Nevertheless, these are based on typically observed changes such as of the reference detector responsivity within a typical one-year recalibration cycle under usual operating conditions at the beamline. Uncertainties for the photon flux can be reduced by applying shorter re-calibration cycles to the reference detectors and shorter measurement cycles for the intensity monitors.

5. Present status and outlook

The possibilities offered at the IDB are quite unique with regards to the availability of undulator radiation in the EUV and VUV regime and the correlated metrological aspects. Besides spectroscopy, the beamline is suited for the radiometric characterization and calibration of complex instrumentation in the relevant spectral ranges, such as space-based radiometers (Reichel *et al.*, 2016; Halain *et al.*, 2018) and photoionization-based detectors for X-ray laser radiation (Tiedtke *et al.*, 2008). The beamline is capable of serving different beam conditions (*e.g.* regarding spot size and absolute photon flux) with the highest spectral purity and known absolute radiometric quantities. Although the radiometric quality regarding the uncertainty in absolute photon-flux

determination is much higher than what is commonly reached for undulator radiation, the uncertainty budget (Table 3) is still too large in comparison with bending-magnet beamlines serving high-end metrological applications (Gottwald *et al.*, 2010). Here, a relative uncertainty better than 1% is to be aspired. Current improvements at the beamline aim at reducing (short-term) thermal instabilities of certain optical components. Improvements in the stability of the intensity monitoring systems (*e.g.* reducing the effects of irradiation degradation of the reference detectors) are also aims as well as improving the performance (pressure stability) of the gas ionization cell for absolute intensity measurements, as this would overcome the reference detector degradation issue.

References

Beckhoff, B. (2008). *J. Anal. At. Spectrom.* **23**, 845–853.

Beckhoff, B., Gottwald, A., Klein, R., Krumrey, M., Müller, R., Richter, M., Scholze, F., Thornagel, R. & Ulm, G. (2009). *Phys. Status Solidi B*, **246**, 1415–1434.

Cimino, R. & Lama, F. (2001). *Nucl. Instrum. Methods Phys. Res. A*, **467–468**, 609–612.

Darlatt, E., Muhsin, B., Roesch, R., Lupulescu, C., Roth, F., Kolbe, M., Gottwald, A., Hoppe, H. & Richter, M. (2016). *Nanotechnology*, **27**, 324005.

Derossi, A., Lama, F., Piacentini, M., Prosperi, T. & Zema, N. (1995). *Rev. Sci. Instrum.* **66**, 1718–1720.

Flechsig, U. (2004). *AIP Conf. Proc.* **705**, 316–319.

Flechsig, U., Patthey, L. & Quitmann, C. (2001). *Nucl. Instrum. Methods Phys. Res. A*, **467–468**, 479–481.

Follath, R. & Senf, F. (1997). *Nucl. Instrum. Methods Phys. Res. A*, **390**, 388–394.

Garcia-Diez, R., Gollwitzer, C. & Krumrey, M. (2015). *J. Appl. Cryst.* **48**, 20–28.

Gottwald, A., Klein, R., Müller, R., Richter, M., Scholze, F., Thornagel, R. & Ulm, G. (2012). *Metrologia*, **49**, S146–S151.

Gottwald, A., Kroth, U., Krumrey, M., Richter, M., Scholze, F. & Ulm, G. (2006). *Metrologia*, **43**, S125–S129.

Gottwald, A., Kroth, U., Richter, M., Schöppe, H. & Ulm, G. (2010). *Meas. Sci. Technol.* **21**, 12510.

Halain, J.-P., *et al.* (2018). *Proc. SPIE*, **10699**, 106990H.

Klein, R., Brandt, G., Fliegauf, R., Hoehl, A., Müller, M., Thornagel, R., Ulm, G., Abo-Bakr, M., Feikes, J., v, Hartrott, M., Holldack, K. & Wüstefeld, G. (2008). *Phys. Rev. ST Accel. Beams*, **11**, 110701.

Kolbe, M., Beckhoff, B., Krumrey, M., Reading, M., van den Berg, J., Conard, T. & de Gendt, S. (2009). *ECS Trans.* **25**, 293–300.

Kramida, A., Ralchenko, Yu., Reader, J. & NIST ASD Team (2014). *NIST Atomic Spectra Database*, Version 5.2. National Institute of Standards and Technology, Gaithersburg, MD, USA (http://physics.nist.gov/asd).

Laubis, C., Barboutis, A., Buchholz, C., Fischer, A., Haase, A., Knorr, F., Mentzel, H., Puls, J., Schönstedt, A., Sintschuk, M., Soltwisch, V., Stadelhoff, C. & Scholze, F. (2016). *Proc. SPIE*, **9776**, 977627.

Lubeck, J., Beckhoff, B., Fliegauf, R., Holfelder, I., Hönicke, P., Müller, M., Pollakowski, B., Reinhardt, F. & Weser, J. (2013). *Rev. Sci. Instrum.* **84**, 045106.

Lüftner, D., Weiß, S., Yang, X., Hurdax, P., Feyer, V., Gottwald, A., Koller, G., Soubatch, S., Puschnig, P., Ramsey, M. G. & Tautz, F. S. (2017). *Phys. Rev. B*, **96**, 125402.

Mercier, B., Compin, M., Prevost, C., Bellec, G., Thissen, R., Dutuit, O. & Nahon, L. (2000). *J. Vac. Sci. Technol. A*, **18**, 2533–2541.

Motz, H., Thon, W. & Whitehurst, R. N. (1953). *J. Appl. Phys.* **24**, 826–833.

Nannarone, S. (2004). *AIP Conf. Proc.* **705**, 450–453.

Neumann, M. D., Cobet, C., Kaser, H., Kolbe, M., Gottwald, A., Richter, M. & Esser, N. (2014). *Rev. Sci. Instrum.* **85**, 055117.

Petersen, H. & Baumgärtel, H. (1980). *Nucl. Instrum. Methods*, **172**, 191–193.

Reichel, T., Gottwald, A., Kroth, U., Laubis, C. & Scholze, F. (2016). *Proc. SPIE*, **9905**, 990547.

Roth, F., Arion, T., Kaser, H., Gottwald, A. & Eberhardt, W. (2018). *J. Electron Spectrosc. Relat. Phenom.* **224**, 84–92.

Roth, F., Herzig, M., Lupulescu, C., Darlatt, E., Gottwald, A., Knupfer, M. & Eberhardt, W. (2015). *J. Appl. Phys.* **118**, 185310.

Roth, F., Lupulescu, C., Arion, T., Darlatt, E., Gottwald, A. & Eberhardt, W. (2014). *J. Appl. Phys.* **115**, 033705.

Roth, F., Lupulescu, C., Darlatt, E., Gottwald, A. & Eberhardt, W. (2016). *J. Electron Spectrosc. Relat. Phenom.* **208**, 2–10.

Schaefer, R., Gottwald, A. & Richter, M. (2018). *J. Phys. B At. Mol. Opt. Phys.* **51**, 135004.

Stellmer, S., Kazakov, G., Schreitl, M., Kaser, H., Kolbe, M. & Schumm, T. (2018). *Phys. Rev. A*, **97**, 062506.

Suits, A. G., Heimann, P., Yang, X., Evans, M., Hsu, C.-W., Lu, K., Lee, Y. T. & Kung, A. H. (1995). *Rev. Sci. Instrum.* **66**, 4841–4844.

Tiedtke, K., Feldhaus, J., Hahn, U., Jastrow, U., Nunez, T., Tschentscher, T., Bobashev, S. V., Sorokin, A. A., Hastings, J. B., Möller, S., Cibik, L., Gottwald, A., Hoehl, A., Kroth, U., Krumrey, M., Schöppe, H., Ulm, G. & Richter, M. (2008). *J. Appl. Phys.* **103**, 094511.

Weiß, S., Lüftner, D., Ules, T., Reinisch, E. M., Kaser, H., Gottwald, A., Richter, M., Soubatch, S., Koller, G., Ramsey, M. G., Tautz, F. S. & Puschnig, P. (2015). *Nat. Commun.* **6**, 8287.